Nanomechanical Proximity Perturbation for Switching in Silicon-Based Directional Couplers for High-Density Photonic Integrated Circuits

Rohit Chatterjee and Chee Wei Wong, *Member, IEEE*

***Abstract*—We describe and demonstrate nanomechanical near-field proximity perturbation for tuning the effective refractive index of silicon-based high-density photonic integrated circuits. The proximity perturbation technique causes an antisymmetric refractive index change in a directional-coupler implementation, enabling switching action from the cross to the bar state. An almost 8-dB extinction ratio with $\sim$14 μs switching speeds is experimentally achieved using this technique with our single-mode waveguides of 500 nm $\times$ 200 nm cross section coupled to a movable 100-nm perturbing dielectric. A practical single-level switch with ring resonators fabricated by CMOS-compatible methods is also demonstrated. [2009-0334]**

***Index Terms*—Microelectromechanical devices, optical directional couplers, optical-waveguide components, photonic switching systems.**

I. Introduction

THE CURRENT drive toward monolithic microphotonics integrated with advanced electronics [1], [2] clearly defines the motivation for silicon-based devices that are capable of performing critical operations. With demonstrations of photonic devices for active channel filters, tunable WDM multiplexers, and dispersion compensators using microring resonators [3]–[7], there exists a need for a hitless switch encompassing these filters. This was demonstrated in a bypass scheme by Haus *et al.* [8]–[11] and Scotti *et al.* [12]. A key component of such a switch is a switched optical directional coupler.

Active optical switching has been achieved using electro-optic effects [13]–[15] or using thermo-optics [16]–[18] to vary the refractive index. However, these devices typically require large electric fields or power (tens of milliwatts) and/or the use of nonlinear materials such as $LiNbO_3$ to achieve the switching, which can present a challenge to chip-scale integration. Recently, switching methods using movable suspended waveguide structures have been proposed. These involve electrostatic switching with significantly lower power switching [19]–[23] but have several micrometer-square cross-sectional areas, which are an order of magnitude larger than our studies. Similar approaches have been examined in [24] and [25] with large extinction ratio, but successful switching was not demonstrated. Related recent works include movable elements with whispering-gallery-mode resonators to switch the coupling [26], [27] or tune the resonances [28]. Our implementation involves a static 2 $\times$ 2 directional coupler with single-mode silicon waveguides, perturbed in the near field by a third movable 100-nm-wide nanoelectromechanical dielectric to effect the switching (as shown in Fig. 1). This allows potentially an antisymmetrically perturbed pair of directional couplers to achieve an optical hitless switch via a π-shifted Mach–Zehnder interferometer with tunable elements [8]–[11].

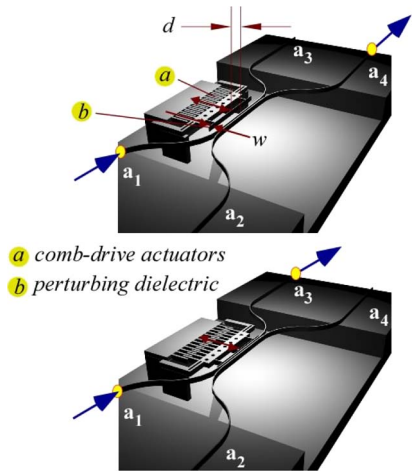

Fig. 1. Schematic of the directional-coupler switch in the unperturbed and perturbed states.

II. Theory

A. Background

We employ coupled-mode theory [29], [30] to examine the device physics in the weakly coupled regime approximation. For two weakly coupled waves with amplitudes a_1 and a_2, the amplitudes are governed by two coupled first-order ordinary differential equations

$$\frac{da_1}{dz} = -j\beta_1 a_1 + \kappa_{12} a_2 \quad (1)$$

$$\frac{da_2}{dz} = -j\beta_2 a_2 + \kappa_{21} a_1 \quad (2)$$

Manuscript received December 31, 2009; accepted January 25, 2010. Date of publication March 22, 2010; date of current version June 3, 2010. This work was supported in part by the Defense Advanced Research Projects Agency Microsystems Technology Office Electronics and Photonics Integrated Circuits program. Subject Editor O. Solgaard.

The authors are with the Optical Nanostructures Laboratory, Center for Integrated Science and Engineering, Solid-State Science and Engineering, and Mechanical Engineering, Columbia University, New York, NY 10027 USA (e-mail: rohit.chatterjee@gmail.com; cww2104@columbia.edu).

Color versions of one or more of the figures in this paper are available online at http://ieeexplore.ieee.org.

Digital Object Identifier 10.1109/JMEMS.2010.2043216

where z is the propagation direction, β_1 and β_2 are the propagation constants, and κ_{12} and κ_{21} are the complex coupling coefficients. The coupling coefficients are evaluated from

$$\kappa_{12} = -\frac{j\omega}{4}\int_{G1}(\varepsilon_1 - \varepsilon)e_2 \cdot e_1^* \, dx\, dy \tag{3}$$

$$\kappa_{21} = -\frac{j\omega}{4}\int_{G2}(\varepsilon_2 - \varepsilon)e_1 \cdot e_2^* \, dx\, dy \tag{4}$$

where e_1 and e_2 are the normalized field amplitudes in waveguides 1 and 2, respectively; x and y are defined in the cross-sectional plane of the waveguides, ε_1 and ε_2 are the permittivities in waveguides 1 and 2, respectively; ε is the background permittivity; and $G1$ and $G2$ are the cross-sectional areas of waveguides 1 and 2, respectively. Each of the waveguides is single mode for the transverse-electric polarization [31]–[33]. An effective propagation constant of the coupled waveguides (β) is found from the determinantal solution of (1) and (2) as

$$\beta = \frac{\beta_1 + \beta_2}{2} \pm \sqrt{\left(\frac{\beta_1 - \beta_2}{2}\right)^2 - \kappa_{12}\kappa_{21}} \tag{5}$$

or

$$\beta = \overline{\beta} \pm (\delta^2 + \kappa_{12}\kappa_{21})^{1/2} = \overline{\beta} \pm \beta_\circ \tag{6}$$

where $\overline{\beta} = (\beta_1 + \beta_2)/2$ and $\beta_\circ = (\delta^2 + \kappa_{12}\kappa_{21})^{1/2}$. δ is the detuning parameter and is defined as $(\beta_1 - \beta_2)/2$. In the weak-coupling assumption, we have $|\kappa_{12}| \ll |\beta_1|$ and $|\beta_2|$; yet, from (5), δ needs to be on the order of κ_{12} for appreciable coupling. Thus, for appreciable coupling, $\beta_1 \cong \beta_2$. To perturb and switch the output ports of a directional coupler, we then need β_1 to be significantly different from β_2. This perturbation can be achieved using a near-field proximity perturbation method described hereinafter. In addition, if waveguides 1 and 2 are identical, we note that $\kappa_{12} = (\beta_+ - \beta_-)/2$, where $\beta_+ = \beta + \beta_\circ$ and $\beta_- = \beta - \beta_\circ$. β_- and β_+ are the lowest symmetric and antisymmetric eigenmodes of the coupled identical waveguides, respectively.

The coupling length for the cross state is of interest. For symmetric waveguides ($\delta = 0$) in a single directional coupler with single excitation ($a_1 = 1$ and $a_2 = 0$), the coupling length for the cross state is found as

$$z_{\text{coupling}} = \frac{\pi}{2\beta_\circ} = \frac{\pi}{\beta_+ - \beta_-} = \frac{\pi}{2\kappa}. \tag{7}$$

If detuning parameter δ equals $\sqrt{3}\kappa$ and we have a single excitation ($a_1 = 1$ and $a_2 = 0$), the power at coupling length z_{coupling} is found to remain in the excitation waveguide instead of crossing over. In effect, the bar state is now achieved by detuning the coupler to $\delta = \sqrt{3}\kappa$. This is shown in Fig. 2, where the power transfer in the cross and the bar port is seen as a function of detuning parameter δ/κ.

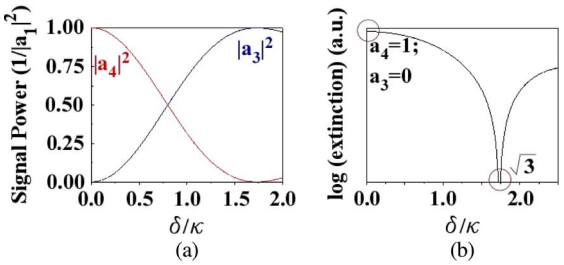

Fig. 2. (a) Power transfer in the cross and the bar port as a function of detuning parameter δ/κ. (b) Extinction ratio as a function of δ/κ.

B. Near-Field Proximity Perturbation

The waveguide effective index is given as a function of the core and cladding indices; it is therefore possible to control the waveguide effective index by modifying the cladding index and thereby control the directional-coupler evanescent coupling and detuning. A method to achieve this detuning is by the introduction of a movable suspended dielectric slab brought into the near-field proximity to one of the arms of the directional coupler, as shown in Fig. 1. The perturbing dielectric in the proximity of the directional coupler causes a change in the effective index, which, in turn, affects the propagation constant, thus affecting the detuning parameter (δ/κ). By tuning the perturbing-dielectric width w and proximity distance d (between the perturbing dielectric and one of the arms of the directional coupler) (as seen in Fig. 1), complete detuning $(\delta = \sqrt{3}\kappa)$ can be achieved with small scattering losses. A similar near-field perturbation technique has also been recently employed to detect nanomechanical motions [34].

C. Comb-Drive Actuation

For switching to take place dynamically, the detuning parameter should switch between 0 and $\sqrt{3}$. Therefore, control needs to be established to bring the perturbing dielectric in close proximity to the directional coupler (to switch to the bar state) and also to move it away from the influence of the evanescent field (to switch to the cross state). Two electrostatic methods of actuation can be used for our purpose. The first method uses electrostatic capacitance plates [27] to pull the perturbing dielectric, while the second method uses comb drives. Either method is feasible, and we simply choose the comb-drive method for implementation. Furthermore, the ease of fabrication and integration with other photonic devices for integrated circuits supports the need for single-level switching (with single-level fabrication) using materials that are compatible with standard CMOS processes. Thus, side proximity perturbation (as opposed to perturbation from the top), as shown in Fig. 1, is implemented with silicon as the material of choice to build these switches. Extensive research has already been done to build comb drives to achieve large displacements with low operating powers and voltages [35]. The dimensions of the comb-fingers, the number of finger pairs, and the spring geometry are the parameters to be considered when dealing with comb-drive actuation, and they directly influence the operating powers. In our device realization, we choose 12 comb-drive fingers, with dimensions of 10-μm length, 1-μm width, and 0.2-μm thickness.

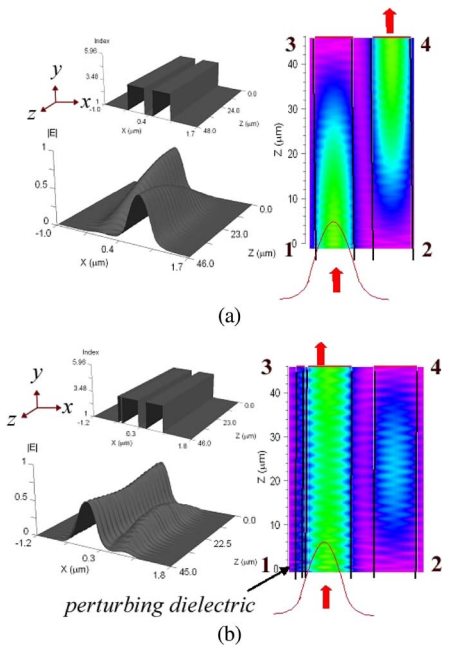

Fig. 3. Full-vectorial BPM results. (a) Index profile of the symmetric directional-coupler arrangement and the power transfer in the unperturbed cross state. (b) Index profile of the symmetric directional coupler with a perturbing slab to achieve the completely detuned state, with the power remaining in the source waveguide at the output plane.

III. Numerical Simulations

Three-dimensional finite-difference time-domain (FDTD) and beam propagation method (BPM) simulation using RSoft [36] was carried out for the directional coupler in both unperturbed and perturbed states. The silicon waveguide dimensions are 500 nm $\times$ 200 nm, and the gap between them is 250 nm. The simulation wavelength is 1550 nm. The BPM results are shown in Fig. 3. In the unperturbed state, it is clearly seen that complete transfer of power takes place from port 1 to port 4 for a waveguide length of 40 μm. With the introduction of a 100-nm-wide perturbing dielectric separated by 80 nm from one of the arms of the directional coupler, no power transfer to port 4 is seen for the same coupling length, and the bar state is achieved.

IV. Design

The design for the directional coupler in both perturbed and unperturbed cases was based on crosstalk minimization. Crosstalk in a directional coupler is defined as the ratio of the power emerging from the untargeted port of the directional coupler to the power emerging from both ports [37]. Thus, in the unperturbed case (see the top panel of Fig. 1), any light emerging from port 3 represents crosstalk, and in the perturbed case (see the bottom panel of Fig. 1), the light emerging from port 4 is the crosstalk. To calculate the crosstalk, the optical powers from ports 3 and 4 are measured, and the crosstalk in decibels is determined from the following: crosstalk (unperturbed) $= 10\log[|a_3|^2/(|a_3|^2+|a_4|^2)]$ and crosstalk (perturbed) $= 10\log[|a_4|^2/(|a_3|^2+|a_4|^2)]$.

First, to determine the complete crossover length for the unperturbed directional couplers, crosstalk minimization was carried out using 3-D FDTD methods. The waveguide cross-sectional height and width dimensions were designed to be the ones typical of a 1550-nm-wavelength high-index-contrast strip silicon-on-insulator waveguide (200 and 500 nm, respectively) in order to guarantee single-mode operation. For a length of 40 μm and 250-nm gap between the waveguides, an almost -21-dB crosstalk (unperturbed) was obtained at 1550 nm (see Fig. 4(b), solid curves). Next, the perturbing-dielectric width $w = 100$ nm, and 200-nm thickness was introduced to one of the arms of the directional coupler. The perturbing-dielectric width was chosen based on scattering-loss calculations using 3-D FDTD methods. The scattering loss for a 100-nm perturbing dielectric at a gap of 80 nm was also calculated and found to be around 0.3 dB and increased to almost 1 dB for 200-nm width due to more significant mode penetration. The crosstalk (perturbed) values at 1550-nm wavelength were then calculated by varying proximity distance d. Fig. 4(a) shows an increase in crosstalk (perturbed) for increasing d with fixed directional-coupler dimensions. This is because an increase in proximity distance makes the perturbing dielectric influence the optical-waveguide mode less. The directional coupler then behaves more in the unperturbed regime, with more signal intensity in port 4. Based on fabrication constraints and crosstalk tradeoffs, a gap of 80 nm was chosen, giving a crosstalk value of -15 dB at 1550 nm. Finally, using this geometry, wavelength tuning was carried out to determine an approximate optimum operating wavelength for both unperturbed and perturbed cases. The results are shown in Fig. 4. Fig. 4(b) shows a minimization of crosstalk at 1550 nm for both unperturbed and perturbed cases. There is a local minimum for crosstalk because the direction coupler length is designed for 1550 nm.

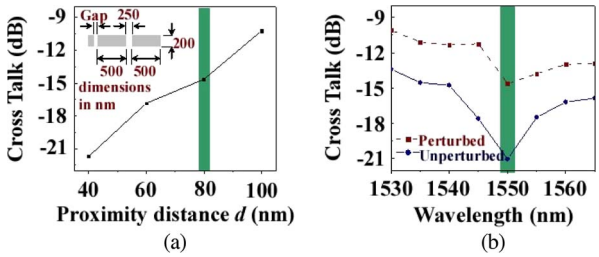

Fig. 4. Design by crosstalk minimization. Results on (a) crosstalk minimization by tuning the gap and (b) crosstalk minimization by wavelength tuning. Note: The highlighted region indicates the selected parameters.

V. Fabrication

The substrate is a silicon-on-insulator wafer, with 205-nm single-crystal device layer on top of a 3 μm buffer oxide layer. Only three major fabrication steps are required to develop the directional-coupler switch. First, deep-UV lithography is used to define the device features, combined with reactive ion etching. Second, electron-beam lithography defines the contact pads for comb-drive actuation. Third, the structures are released by an isotropic buffered oxide wet etch. The SEM results are shown in Fig. 5, where the bottom-right panel shows a perturbing dielectric with 100-nm width at a gap of 150 nm from the directional couplers.

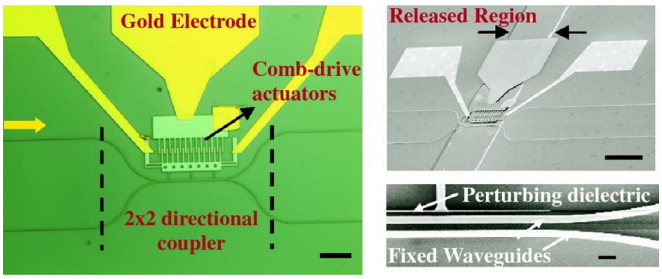

Fig. 5. (Left) Optical micrograph image of the single-level NEMS switch showing the different components. Scale bar: 20 μm. (Top right) SEM of the fabricated switch showing the region around the directional coupler that has been released to allow movement of the comb drives. Scale bar: 50 μm. (Bottom right) Zoomed-in SEM photograph showing the perturbing dielectric and the fixed waveguides. A gap of $\sim$150 nm is achieved between the perturbing dielectric and one of the arms of the directional couplers. Scale bar: 500 nm.

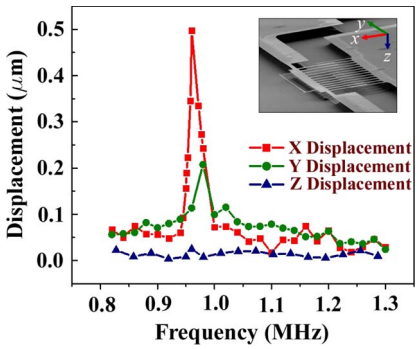

Fig. 6. Frequency response of the comb drives with a dc-biased sinusoid at 5 V peak to peak and 50-V bias.

VI. Experiments

First, the dynamical response of the system was characterized with the micromotion analyzer at the Freeman group at MIT. A dc-biased sinusoid (5 V peak to peak and 50-V bias) was applied to the movable combs while the fixed combs were grounded. The frequency response (Fig. 6) shows a maximum displacement of around 500 nm at resonance, which is enough to move the perturbing dielectric away from the influence of the optical field in the waveguide, making the switch behave in the unperturbed state. The figure also shows that the motions in the other directions are relatively suppressed, with negligible out-of-plane displacement at the operating resonance frequency.

Next, the entire switch (see Fig. 5) was fabricated and then tested using the setup shown in Fig. 7(a). A tunable laser source (tunable from 1480 to 1580 nm) served as the input source. Tapered lensed fibers were used for input and output coupling to the chip. The output light was sent to an InGaAs photodiode and read out using a lock-in amplifier. DC drive voltages from 5 to 40 V were applied between the fixed and movable parts of the actuator. The bar-state transmission was measured with and without the application of dc drive voltage at 1550 nm. The result for the switching action is shown in Fig. 7(b). Almost 8 dB of transmission drop can be seen with the application of 40 V dc. Between 30 and 40 V, no appreciable change in transmission is observed, indicating that the perturbing dielectric is sufficiently far from the waveguide evanescent field and does not affect the propagation constants. From these data, the

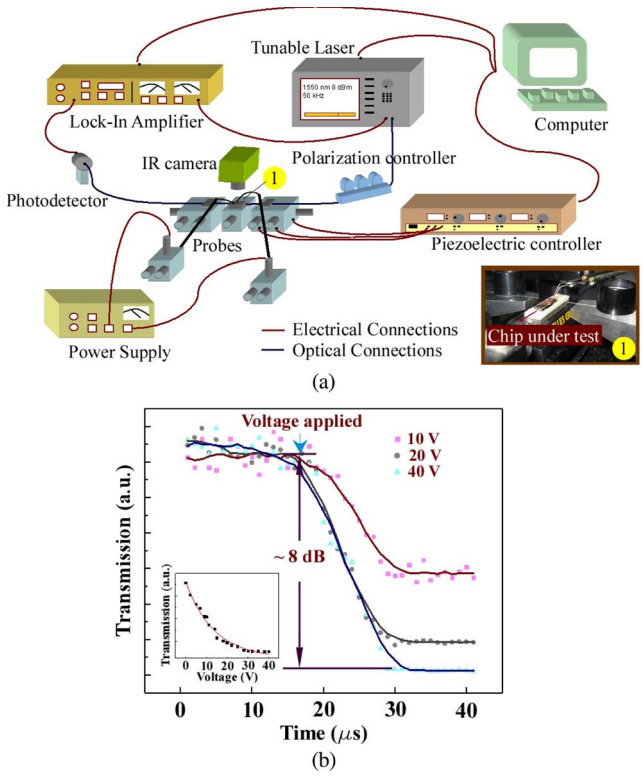

Fig. 7. Experiments on the switch. (a) Experimental setup for the dynamic measurements of the switch. (b) Bar-state optical transmission as a function of time for varying voltages. (Inset) Average bar-state transmission as a function of voltage. A first-order exponential is fitted to the experimental data.

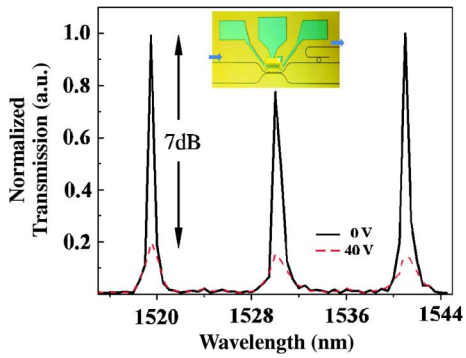

Fig. 8. Drop-port transmission of a ring resonator placed after the switch when 0 and 40 V are applied to the switch. The inset shows an optical image of the device under test.

90%–10% switching speed can be estimated to be $\sim$14 μs. The change in average optical transmission with applied voltage is shown in the inset of Fig. 7(b). As expected, because of the evanescent decay of the mode away from the waveguides, the measured transmission decreases rapidly with increasing voltage when pulling away the perturbing dielectric. The excess loss, i.e., the additional loss on top of the fiber-chip coupling losses, was also quantified to be less than 1 dB.

To further confirm the practicability of the switch, microring resonators [38] (with a ring diameter of 14.2 μm and a waveguide coupling gap of 0.2 μm) were fabricated along with the switch, as shown in the inset of Fig. 8, toward a reconfigurable optical filter. The drop-port transmission is shown in Fig. 8. The solid black curve corresponds to the state when no

voltage is applied to the switch, and the dashed red curve shows the transmission when 40 V dc is applied to the switch. We observe an almost 7-dB extinction ratio in the transmission in the drop port of the ring resonator between the ON and OFF states of the switch. The transmission attenuation is enabled with the actuation of the 100-nm perturbing dielectric away from the evanescent field of the directional coupler, resulting in the cross state of the directional coupler with signal exiting from the port without the microring resonators. The extinction ratio is currently at 7 dB due to fabrication imperfections, where the gaps between the perturbing dielectric and the waveguide are around 150 nm. However, with current improved fabrication tolerances where the desired gaps of 80 nm or less are achievable, we expect that an improved extinction ratio of more than 20 dB can be obtained.

VII. Conclusion

We have demonstrated the near-field proximity perturbation technique for integrated photonic switching in silicon-based directional couplers, with potential toward a hitless bypass scheme for optical communications. An almost 8-dB switching action with $\sim 14\ \mu$s switching speeds from the bar to the cross state for directional couplers has been obtained at 40 V for transparent wavelength switching. The application of the switch with an optical ring resonator has also been presented, where a 7-dB switching action has been found.

Acknowledgment

The authors would like to thank M. Popovic, M. Watts, L. C. Kimerling, and X. Yang for the helpful discussions; S. Desai and D. Freeman for generously allowing the use of the micromotion analyzer; and A. Stein, M. Yu, and D.-L. Kwong for the fabrication contributions.

References

[1] L. C. Kimerling, L. Dal Negro, S. Saini, Y. Yi, D. Ahn, S. Akiyama, D. Cannon, J. Liu, J. G. Sandland, D. Sparacin, J. Michel, K. Wada, and M. R. Watts, "Monolithic silicon microphotonics," in *Silicon Microphotonics*, L. Pavesi and D. J. Lockwood, Eds. New York: Springer-Verlag, 2004, ch. 3.

[2] G. Masini, L. Colace, and G. Assanto, "Si based optoelectronics for communications," *Mater. Sci. Eng. B*, vol. 89, no. 1–3, pp. 2–9, Feb. 2002.

[3] D. R. Lim, B. E. Little, K. K. Lee, M. Morse, H. H. Fujimoto, H. A. Haus, and L. C. Kimerling, "Micron-size channel dropping filters using silicon waveguide devices," *Proc. SPIE*, vol. 3847, pp. 65–71, 1999.

[4] B. E. Little, J. S. Foresi, G. Steinmeyer, E. R. Thoen, S. T. Chu, H. A. Haus, E. P. Ippen, L. C. Kimerling, and W. Greene, "Ultra-compact Si–SiO2 microring resonator optical channel dropping filters," *IEEE Photon. Technol. Lett.*, vol. 10, no. 4, pp. 549–551, Apr. 1998.

[5] S. C. Hagness, D. Rafizadeh, S. T. Ho, and A. Taflove, "FDTD microcavity simulations: Design and experimental realization of waveguide-coupled single-mode ring and whispering-gallery-mode disk resonators," *J. Lightw. Technol.*, vol. 15, no. 11, pp. 2154–2165, Nov. 1997.

[6] G. Lenz and C. K. Madsen, "General optical all-pass filter structures for dispersion control in WDM systems," *J. Lightw. Technol.*, vol. 17, no. 7, pp. 1248–1254, Jul. 1999.

[7] P. P. Absil, J. V. Hryniewicz, B. E. Little, P. S. Cho, R. A. Wilson, L. G. Joneckis, and P. T. Ho, "Wavelength conversion in GaAs micro-ring resonators," *Opt. Lett.*, vol. 25, no. 8, pp. 554–556, Apr. 2000.

[8] H. A. Haus, M. A. Popovic, and M. R. Watts, "Broadband hitless bypass switch for integrated photonic circuits," *IEEE Photon. Technol. Lett.*, vol. 18, no. 10, pp. 1137–1139, May 2006.

[9] M. A. Popović, T. Barwicz, M. S. Dahlem, F. Gan, C. W. Holzwarth, P. T. Rakich, M. R. Watts, H. I. Smith, F. X. Kärtner, and E. P. Ippen, "Hitless-reconfigurable and bandwidth-scalable silicon photonic circuits for telecom and interconnect applications," presented at the Optical Fiber Conf., San Diego, CA, 2008, Paper OTuF4.

[10] M. A. Popović, E. P. Ippen, and F. X. Kärtner, "Universally balanced photonic interferometers," *Opt. Lett.*, vol. 31, no. 18, pp. 2713–2715, Sep. 2006.

[11] H. A. Haus, M. A. Popovic, and M. R. Watts, "General approach to hitless switching and FSR extension resonators in integrated photonic circuits," presented at the Optical Fiber Conf., Anaheim, CA, 2006, Paper OWI66.

[12] R. E. Scotti, C. K. Madsen, C. H. Henry, G. Lenz, Y. P. Li, H. Presby, and A. White, "A hitless reconfigurable add-drop multiplexer for WDM networks utilizing planar waveguides, thermo-optic switches and UV-induced gratings," in *Proc. Opt. Fiber Conf.*, 1998, pp. 142–143.

[13] H. Kogelnik and R. V. Schmidt, "Switched directional couplers with alternating $\Delta\beta$," *IEEE J. Sel. Topics Quantum Electron.*, vol. STQE-12, no. 7, pp. 396–401, Jul. 1976.

[14] R. A. Soref and B. R. Bennett, "Electrooptical effects in silicon," *IEEE J. Sel. Topics Quantum Electron.*, vol. STQE-23, no. 1, pp. 123–129, Jan. 1987.

[15] R. S. Jacobsen, K. N. Andersen, P. I. Borel, J. Fage-Pedersen, L. H. Frandsen, O. Hansen, M. Kristensen, A. V. Lavrinenko, G. Moulin, H. Ou, C. Peucheret, B. Zsigri, and A. Bjarklev, "Strained silicon as a new electro-optic material," *Nature*, vol. 441, no. 7090, pp. 199–202, May 2006.

[16] Q. Lai, W. Hunziker, and H. Melchior, "Low-power compact 2×2 thermooptic silica-on-silicon waveguide switch with fast response," *IEEE Photon. Technol. Lett.*, vol. 10, no. 5, pp. 681–683, May 1998.

[17] R. L. Espinola, M. C. Tsai, J. T. Yardley, and R. M. Osgood, Jr., "Fast and low-power thermooptic switch on thin silicon-on-insulator," *IEEE Photon. Technol. Lett.*, vol. 15, no. 10, pp. 1366–1368, Oct. 2003.

[18] W. M. J. Green, H. F. Hamann, L. Sekaric, M. J. Rooks, and Y. A. Vlasov, "Ultra-compact reconfigurable silicon optical devices using micron-scale localized thermal heating," in *Proc. Opt. Fiber Commun. Conf. Expo. Nat. Fiber Optic Eng. Conf.*, 2007, pp. 604–606.

[19] E. Ollier, "Optical MEMS devices based on moving waveguides," *IEEE J. Sel. Topics Quantum Electron.*, vol. 8, no. 1, pp. 155–162, Jan./Feb. 2002.

[20] T. Bakke, C. P. Tigges, J. J. Lean, C. T. Sullivan, and O. B. Spahn, "Planar microoptomechanical waveguide switches," *IEEE J. Sel. Topics Quantum Electron.*, vol. 8, no. 1, pp. 64–72, Jan./Feb. 2002.

[21] M. W. Pruessner, K. Amarnath, M. Datta, D. P. Kelly, S. Kanakaraju, P.-T. Ho, and R. Ghodssi, "InP-based optical waveguide MEMS switches with evanescent coupling mechanism," *J. Microelectromech. Syst.*, vol. 14, no. 5, pp. 1070–1081, Oct. 2005.

[22] E. Bulgan, Y. Kanamori, and K. Hane, "Submicron silicon waveguide optical switch driven by microelectromechanical actuator," *Appl. Phys. Lett.*, vol. 92, no. 10, pp. 101 110-1–101 110-3, Mar. 2008.

[23] M. C. Wu, J. Yao, and M.-C. Lee, "Silicon microresonators with MEMS-actuated tunable couplers," in *Proc. 4th IEEE Int. Conf. Group IV Photon.*, 2007, pp. 43–45.

[24] F. Chollet, M. de Labachelerie, and H. Fujita, "Compact evanescent optical switch and attenuator with electromechanical actuation," *IEEE J. Sel. Topics Quantum Electron.*, vol. 5, no. 1, pp. 52–59, Jan./Feb. 1999.

[25] G. J. Veldhuis, T. Nauta, C. Gui, J. W. Berenschot, and P. V. Lambeck, "Electrostatically actuated mechanooptical waveguide ON–OFF switch showing high extinction at a low actuation-voltage," *IEEE J. Sel. Topics Quantum Electron.*, vol. 5, no. 1, pp. 60–66, Jan./Feb. 1999.

[26] M.-C. M. Lee and M. C. Wu, "Tunable coupling regimes of silicon microdisk resonators using MEMS actuators," *Opt. Express*, vol. 14, no. 11, pp. 4703–4712, May 2006.

[27] M.-C. M. Lee and M. C. Wu, "MEMS-actuated microdisk resonators with variable power coupling ratios," *IEEE Photon. Technol. Lett.*, vol. 17, no. 5, pp. 1034–1036, May 2005.

[28] G. N. Nielson, D. Seneviratne, F. Lopez-Royo, P. T. Rakich, Y. Avrahami, M. R. Watts, H. A. Haus, H. L. Tuller, and G. Barbastathis, "Integrated wavelength-selective optical MEMS switching using ring resonator filters," *IEEE Photon. Technol. Lett.*, vol. 17, no. 6, pp. 1190–1192, Jun. 2005.

[29] H. A. Haus, *Waves and Fields in Optoelectronics*. Englewood Cliffs, NJ: Prentice-Hall, 1983.

[30] A. Yariv, *Optical Electronics,* 4th ed. Philadelphia, CA: Saunders, 1991.

[31] T. Chu, H. Yamada, S. Nakamura, M. Tojo, Y. Urino, S. Ishida, and Y. Arakawa, "Silicon photonic-wire waveguide devices," *Proc. SPIE*, vol. 6477, pp. 647 709-1–647 709-9, Feb. 2007.

[32] H. Yamada, T. Chu, S. Nakamura, Y. Urino, S. Ishida, and Y. Arakawa, "Si waveguide devices for optical communication," in *Proc. Conf. Lasers Electro Optics Pacific Rim Conf. Lasers Electro-Optics*, 2007, pp. 216–217.

[33] H. Yamada, T. Chu, S. Ishida, and Y. Arakawa, "Si photonic wire waveguide devices," *IEEE J. Sel. Topics Quantum Electron.*, vol. 12, no. 6, pp. 1371–1379, Nov./Dec. 2006.
[34] I. D. Vlaminck, J. Roels, D. Taillaert, D. V. Thourhout, R. Baets, L. Lagae, and G. Borghs, "Detection of nanomechanical motion by evanescent light wave coupling," *Appl. Phys. Lett.*, vol. 90, no. 23, p. 233 116, Jun. 2007.
[35] R. Legtenberg, A. W. Groeneveld, and M. Elwenspoek, "Comb-drive actuators for large displacements," *J. Micromech. Microeng.*, vol. 6, no. 3, pp. 320–329, Sep. 1996.
[36] Rsoft Design Group, Inc., Ossining, NY.
[37] J. C. Powelson, W. Feng, S. Lin, R. J. Feuerstein, and D. Tomic, "Crosstalk of passive directional couplers," *J. Lightw. Technol.*, vol. 16, no. 11, pp. 2020–2027, Nov. 1998.
[38] Y. A. Vlasov, F. Xia, S. Assefa, and W. Green, "Silicon micro-resonators for on-chip optical networks," in *Proc. Quantum Electron. Laser Sci. Conf.*, 2008, p. 2.

Rohit Chatterjee received the Ph.D. degree (with distinction) from the Optical Nanostructures Laboratory, Department of Mechanical Engineering, Columbia University, New York, NY, in 2008.

His research interests include silicon nanophotonics, including waveguide- and photonic-crystal-based devices, nanoelectromechanical systems, and nanofabrication.

Dr. Chatterjee is a member of the American Physical Society.

Chee Wei Wong (M'03) received the B.Sc. degree (with highest honors) in mechanical engineering and the B.A. degree (with highest honors) in economics from the University of California, Berkeley, in 1999, and the M.S. and D.Sc. degrees in mechanical engineering (optical nanotechnology) from the Massachusetts Institute of Technology (MIT), Cambridge, in 2001 and 2003, respectively.

He was a Postdoctoral Research Associate in the MIT Microphotonics Center in 2003. Since 2004, he has been with Columbia University, New York, NY, where he is currently a faculty member. He enjoys working on nonlinear and quantum optics in nanophotonics, silicon electronic–photonic circuits and photonic crystals, quantum-dot interactions in nanocavities, nanoelectromechanical systems, and nanofabrication.

Dr. Wong is a member of the American Physical Society, the American Society of Mechanical Engineers, the Optical Society of America (OSA), and Sigma Xi. He received the 2009 3M Faculty Award, a 2008 National Science Foundation CAREER Award, and a 2007 Defense Advanced Research Projects Agency Young Faculty Award.